Journal of Alloys and Compounds 509 (2011) 5466–5471

Contents lists available at ScienceDirect

Journal of Alloys and Compounds

journal homepage: www.elsevier.com/locate/jallcom

Deuterium absorption in $Mg_{70}Al_{30}$ thin films with bilayer catalysts: A comparative neutron reflectometry study

Eric Poirier[a,1], Chris T. Harrower[b], Peter Kalisvaart[b], Adam Bird[a], Anke Teichert[c,d,e], Dirk Wallacher[c], Nico Grimm[c], Roland Steitz[c], David Mitlin[b], Helmut Fritzsche[a,*]

[a] National Research Council Canada/Canadian Neutron Beam Centre, Bldg. 459, Chalk River Laboratories, Chalk River, ON, K0J 1J0, Canada
[b] Chemical and Materials Engineering, University of Alberta and National Research Council Canada/National Institute for Nanotechnology, Edmonton, AB, T6G 2M9, Canada
[c] Helmholtz Zentrum Berlin, Hahn-Meitner-Platz 1, 14109 Berlin, Germany
[d] Instituut voor Kern-en Stralingsfysica and INPAC, K.U. Leuven, Celestijnenlaan 200D, B-3001 Leuven, Belgium
[e] Laboratorium voor Vaste-Stoffysica en Magnetisme and INPAC, K.U. Leuven, Celestijnenlaan 200D, B-3001 Leuven, Belgium

ARTICLE INFO

Article history:
Received 6 January 2011
Accepted 19 February 2011
Available online 24 February 2011

Keywords:
Thin films
Metal hydrides
Neutron reflectometry
Catalysts

ABSTRACT

We present a neutron reflectometry study of deuterium absorption in thin films of Al-containing Mg alloys capped with a Ta/Pd, Ni/Pd and Ti/Pd-catalyst bilayer. The measurements were performed at room temperature over the 0–1 bar pressure range under quasi-equilibrium conditions. The modeling of the measurements provided a nanoscale representation of the deuterium profile in the layers at different stages of the absorption process. The absorption mechanism observed was found to involve spillover of atomic deuterium from the catalyst layer to the Mg alloy phase, followed by the deuteration of the Mg alloy. Complete deuteration of the Mg alloy occurs in a pressure range between 100 and 500 mbar, dependent on the type of bilayer catalyst. The use of a Ti/Pd bilayer catalyst yielded the best results in terms of both storage density and kinetic properties.

1. Introduction

Hydrogen-powered vehicles are foreseen as the ultimate solution to mitigate environmental impacts associated with transportation needs. Their practicality, however, depends on the development of a high capacity hydrogen storage system that can be charged quickly and efficiently at moderate pressures and temperatures (*P*,*T*). A hydrogen fuel-cell vehicle meeting these criteria could offer the advantages of electrical propulsion, while reaching ranges and refueling times comparable to gasoline vehicles. As part of the ongoing research on solid state hydrogen storage, absorption in Mg alloys have attracted a lot of interest. Mg offers high gravimetric and volumetric hydrogen densities, as well as a low cost due to its abundance. One of the main issues with Mg is the high operating temperatures (~300 °C) required for fast kinetics during absorption and desorption [1]. Therefore, recent efforts have focused on the addition of catalysts, formation of nanocrystalline phases (e.g. by ball-milling), and destabilization agents in order to improve the kinetics, and possibly the thermodynamics of hydrogen absorption [2–4]. The effectiveness of these approaches can be better assessed when a detailed nanoscale representation of the system is available. In that respect, thin Mg films constitute very interesting model systems to study fundamentals of absorption and catalysis as they can be synthesized with nanoscale layers of specific composition and dimension. Their synthesis, under well-controlled conditions, also minimizes detrimental contamination and surface oxidation.

It is well-known that a Pd layer improves the kinetics of hydrogen absorption in many metals [5–8] including thin MgAl films [9]. The Pd layer prevents the formation of an oxide layer, and is likely to lower hydrogen dissociation and diffusion barriers prompting atomic hydrogen spillover into the bulk hydrogen absorbing phase [10]. Improvement is achieved through a two-step mechanism involving absorption in the Pd layer and subsequent spillover in the main phase. This mechanism was evidenced by neutron reflectometry (NR) measurements on catalyzed $Mg_{70}Al_{30}$ thin films at room temperature and low pressure (<1.3 bar) [11]. The same NR experiments also revealed depletion zones near the $Mg_{70}Al_{30}$ interfaces, which were attributed to the elastic connection between the Mg alloy and adjacent layers. Deuterium concentration up to 5 wt.% was found in the $Mg_{70}Al_{30}$ layer, a significant value under these very mild conditions. At elevated temperatures Pd tends to form an alloy with the underlying Mg phase that hinders or prevents further hydrogen absorption. In order to reduce Pd alloying, the introduction of Fe, Ti or Ta interlayer underneath the Pd cap to form a bilayer catalyst has been considered [12–14]. Interestingly, the use of 5 nm Ta/5 nm Pd bilayer catalyst was also found to decrease the desorption temperature [14], and to improve the

* Corresponding author. Tel.: +1 613 584 8811x43711; fax: +1 613 584 4040.
E-mail address: Helmut.Fritzsche@nrc-cnrc.gc.ca (H. Fritzsche).
[1] Present address: General Motors Co./Optimal Inc., Chemical Sciences and Materials Systems Laboratory, Mail Code 480-102-000, 30500 Mound Rd., Warren, MI 48090-9055, United States.

0925-8388/$ – see front matter
doi:10.1016/j.jallcom.2011.02.111

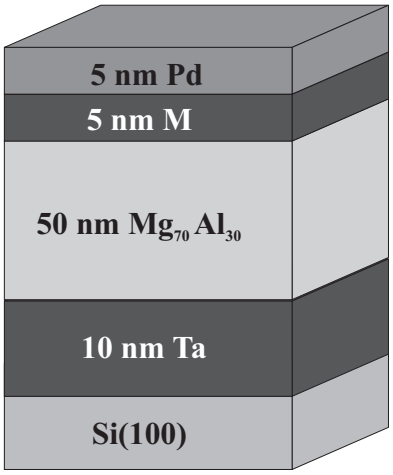

Fig. 1. Schematic of a film's structure; the symbol M in the top bilayer stands for Ta, Ni or Ti.

absorption rate at low pressures [11]. The improved kinetics at low pressure was attributed to a reduction of the nucleation barrier for the deuteration of the Mg alloy layer [11]. Similarly, the addition of metal interlayer was found to improve to various degrees the cyclability [13], and the kinetics [13,15]. The kinetics, in particular, was also found to depend on the enthalpy of solution (or formation) and thickness of the metallic interlayer, as found on interlayers exceeding 30 nm [15]. It should be pointed out that the use of a bilayer catalyst will affect the gravimetric storage capacity and materials costs as well. In this context, it appears important to get a better understanding of the mechanism by which minimal (5 nm M/5 nm Pd) bilayer catalysts involving different metals (M) could influence absorption properties.

In this report, we present NR measurements made on catalyzed $Mg_{70}Al_{30}$ thin films absorbing deuterium under quasi-equilibrium conditions. The measurements were performed in situ, at room temperature and over a 0–1 bar D_2 pressure range. NR is a powerful tool to determine the deuterium concentration profiles in the various layers with nanometer resolution [14,16,17]. The NR experiments were conducted on $Mg_{70}Al_{30}$ alloy films with catalyst bilayers containing M = Ta, Ni and Ti in order to investigate specifically the effect of these metals. A composition of 70 at.% Mg and 30 at.% Al was used as it was previously found to be optimal with respect to both capacity and kinetics [16,17]. Aluminum may also reduce the stability of the hydride, leading to improved dehydrogenation conditions [18,19]. We used X-ray reflectometry (XRR) to verify the film structure following the in situ NR measurements. XRR is a valuable complementary technique as it is not sensitive to deuterium and therefore provides information on the position of the metal atoms, i.e. metal interdiffusion.

2. Experimental

2.1. Sample preparation

The thin film samples used in this study were fabricated by co-sputtering onto a (1 0 0) silicon wafer in a confocal sputtering chamber (Orion 5 instrument from AJA International) operating at an Ar (purity 99.999% pure) pressure of 5×10^{-3} mbar, which had been previously evacuated to a pressure less than 3×10^{-8} mbar. The oxide was removed in situ by reverse etching the native oxide prior to film depositions. First a 10 nm Ta layer was deposited onto the wafer and, without interruption, a 50 nm $Mg_{70}Al_{30}$ layer was co-sputtered followed by 5 nm Ta (or Ni, Ti) and a 5 nm Pd top layer. The film structure is represented in Fig. 1.

2.2. In situ neutron reflectometry

The NR experiments were performed on the V6 horizontal reflectometer at the Helmholtz Zentrum, Berlin. This instrument is operated using a 0.466 nm neutron wavelength. The instrument involves an aluminum sample cell, allowing for in situ gas absorption measurements. The measurements were performed at room temperature, from a deuterium pressure of 1 mbar up to 1 bar, using ultra high purity deuterium (99.999%). Absorption under these mild conditions is relatively slow, allowing for quasi-equilibrium absorption measurements. Consequently, such NR experiments uniquely capture the evolution of the deuterium concentration profile during the absorption process, allowing for a detailed, i.e. nanoscale, representation of the absorption mechanism. This hydrogen profiling is usually not possible with other techniques, either at high temperature and/or on powder samples.

The NR reflectivity curves were measured in a specular configuration, i.e. with the interface of the films perpendicular to the scattering vector q_z. In this configuration, the neutron interaction with the films is reduced to a one-dimensional problem that can be described with a neutron index of refraction n analogous to optical reflectivity. The value of n depends on the strength of the interaction of neutrons with specific isotopes in the films and is given by [20]:

$$n = \sqrt{1 - \frac{\lambda^2}{\pi} N_j b_j} \tag{1}$$

where λ is the neutron wavelength, N_j is the number density, b_j is the coherent nuclear scattering length, and the product $N_j b_j = S$ is the scattering length density (SLD) in layer j. The SLD depends on the elements and their isotopes present in the sample. Deuterium is used because of its large coherent scattering length, which leads to a significant increase in the layers' SLD upon absorption. The measured reflectometry curves were analyzed using the *Motofit* software involving genetic optimization with least square [21,22]. The analysis was performed using slab models, containing four to seven layers. The measured data were fitted by the models by varying the SLD, layer thickness, and interface roughness of each individual layer j. Total neutron reflection occurs up to a critical angle, or scattering vector q_c. The latter depends on the average scattering length density $\bar{S}$ of the materials such as [20]:

$$q_c = \frac{4\pi}{\lambda} \sin\theta_c = 4\sqrt{\pi \bar{S}} \tag{2}$$

This implies the critical edge angle increases as a result of deuterium absorption. Corresponding displacements of q_c were measured in short scans to quickly estimate the average amount of deuterium absorbed and identify quasi-equilibrium conditions. Typically, measurements over the $q = 0 - 0.5\ \mathrm{nm}^{-1}$ range were assumed in quasi-equilibrium when the critical edge, or the full NR curve, showed no major changes over a 1–2 h measurement period. Some measurements not satisfying this condition could not be fitted and were discarded. The deuterium content in each layer can be estimated from the scattering length density using the expression [6]:

$$C_D \cong \left[\frac{S_{M+D}}{S_{M(p=0)}} \frac{t_{M+D}}{t_M} - 1 \right] \frac{b_M}{b_D} \tag{3}$$

where S_{M+D} is the scattering length density of the deuterium-charged layer, $S_{M(p=0)}$ is the scattering length density of the layer in absence of deuterium, t_{M+D} and t_M are the corresponding thicknesses, and b_M and b_D are the scattering length of the metal and deuterium respectively.

2.3. X-ray measurements

X-ray reflectometry and diffraction measurements were also performed to confirm the structure and composition of the samples. These measurements were performed about 60 days following the NR measurements and hence, give some information on the stability of the absorbed phases. The measurements were made with a commercial Rigaku Ultima III X-ray diffractometer used in a high resolution configuration with the Cu $K_{\alpha 1}$ wavelength of 0.15406 nm.

3. Results

3.1. Neutron reflectometry

3.1.1. $Mg_{70}Al_{30}$/Ta/Pd

Neutron reflectivity curves and SLD profiles on the $Mg_{70}Al_{30}$/Ta/Pd sample are shown in Fig. 2. The corresponding SLD profiles, i.e. the SLD as a function of the direction z parallel to the surface normal of the film, are displayed in the insets. These insets provide a real space representation of the film. Fig. 2a refers to the as-prepared sample, as measured in air. The curve exhibits the characteristic Kiessig fringes associated with multiple reflections [23]. It was successfully fit using a four layers model. The scattering length density and the thickness of the $Mg_{70}Al_{30}$ phase are $2.2 \times 10^{-4}\ \mathrm{nm}^{-2}$ and 54 nm, respectively. The SLD corresponds to the value calculated from tabulated data ($2.2 \times 10^{-4}\ \mathrm{nm}^{-2}$) and the measured thickness is within 10% of the expected value (~50 nm). Following this measurement, deuterium was slowly

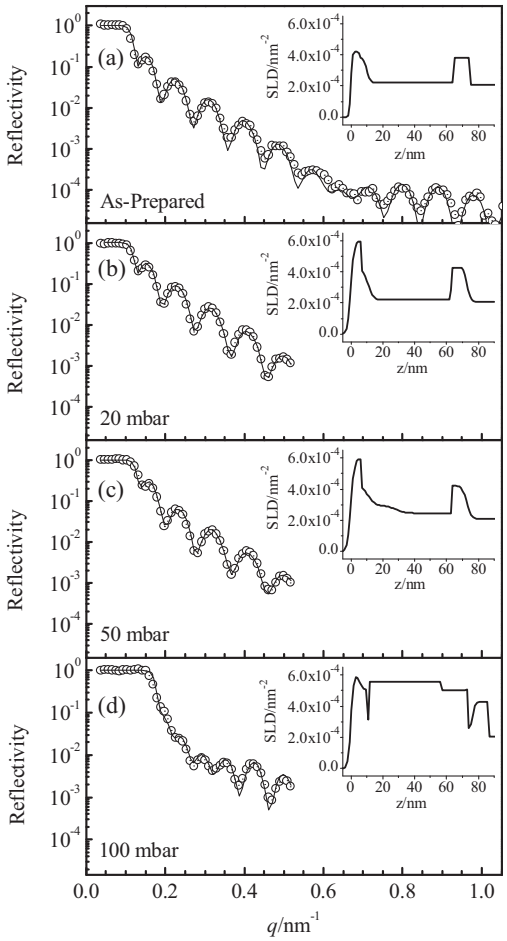

Fig. 2. Neutron reflectivity curves and corresponding SLD profiles on the Ta/$Mg_{70}Al_{30}$/Ta/Pd sample: (a) as prepared, and at D_2 pressures of: (b) 20 mbar, (c) 50 mbar, and (d) 100 mbar.

introduced into the sample cell and measurements were performed at different pressures. Fig. 2b represents the reflectivity curve measured at a D_2 pressure of 20 mbar. The SLD profile shows an increase of the SLD for both, the top and bottom layers, while the SLD of the $Mg_{70}Al_{30}$ layer remains essentially unchanged. From that we can conclude that both, the top and bottom layers, contain deuterium, while the $Mg_{70}Al_{30}$ phase contains virtually none. Further increase in the D_2 pressure up to 50 mbar (Fig. 2c) resulted in some deuterium absorption in the $Mg_{70}Al_{30}$ phase. The latter exhibits a deuterium concentration gradient as illustrated by the varying SLD profile in this layer over the ~10–20 nm range. Note that a fifth layer had to be introduced within the $Mg_{70}Al_{30}$ phase to fit the NR curve at this point. As will be shown later, such gradient is not due to changes in the $Mg_{70}Al_{30}$/Ta/Pd layer structure, but most likely results from the slow evolution of the deuterium concentration under these very mild (P,T) conditions. The average SLD in the $Mg_{70}Al_{30}$ phase is 2.6×10^{-4} nm^{-2}, and the corresponding deuterium-to-metal ratio, as calculated using Eq. (3), is $D/M = 0.09$. At a pressure of 100 mbar (Fig. 2d) dramatic changes are apparent in both, the reflectivity curve and the SLD profile which reveal the quasi saturation of the main $Mg_{70}Al_{30}$ phase. The SLD profile in the $Mg_{70}Al_{30}$ layer also shows, at 100 mbar, a reduced gradient with an average value of about 5.3×10^{-4} nm^{-2}, which corresponds to $D/M = 1.26$. The sample absorbs most of the deuterium (~90% of the maximum value) at this pressure within about 7.5 h, as revealed by the evolution of the critical edge shown in Fig. 3. Further increases over the 500–1000 mbar range lead to

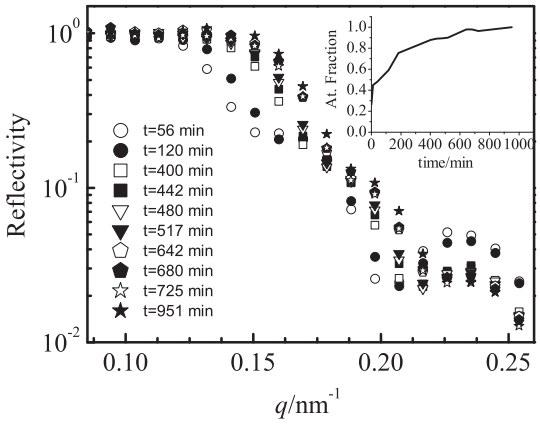

Fig. 3. Neutron reflectivity curves measured on Ta/$Mg_{70}Al_{30}$/Ta/Pd showing the evolution of the critical edge region at 100 mbar. The sample absorbed most of the deuterium after about 7.5 h as shown in the inset.

incremental changes in both, the SLDs and thickness of the layers (not shown) indicating the sample was already close to saturation. Near saturation (Fig. 2d), the reflectivity curve was fit with a seven layers model involving small gaps of about 1–2 nm on each side of the $Mg_{70}Al_{30}$ phase. These two gaps, which will be discussed later, had to be introduced in the model at this point; otherwise the measured curves could not be fit correctly as shown in Fig. 4. The $Mg_{70}Al_{30}$ layer ultimately reaches an average SLD of about 5.55×10^{-4} nm^{-2}, and at a thickness of about 67 nm revealing a 23% expansion. The corresponding deuterium absorption in the $Mg_{70}Al_{30}$ phase reaches a ratio of $D/M = 1.3$, or the equivalent of 5 wt.%. This value is about 20% higher than the 4.1 wt.%, reported previously [17], a likely result of the in situ approach, which prevents partial desorption of deuterium in air.

3.1.2. $Mg_{70}Al_{30}$/Ni/Pd

Reflectivity curves and SLD profiles of the $Mg_{70}Al_{30}$/Ni/Pd sample are presented in Fig. 5 for various D_2 pressures. Fig. 5a shows the reflectivity curves as well as the corresponding SLD for the as-prepared sample. As for the previous sample, SLD values were found in agreement with expected ones from tabulated data. The high SLD observable around 5 nm is due to the presence of Ni, which has a large coherent scattering length. Following deuterium exposure over the 20–50 mbar range (Fig. 5b and c), the sample absorbs deuterium mainly in the top Pd layer, as well as in the bottom Ta layer to a smaller extent. Negligible amounts of deuterium are found in the main $Mg_{70}Al_{30}$ phase at this point. Significant absorption in the $Mg_{70}Al_{30}$ layer is observable at 500 mbar (Fig. 5d). At this pressure,

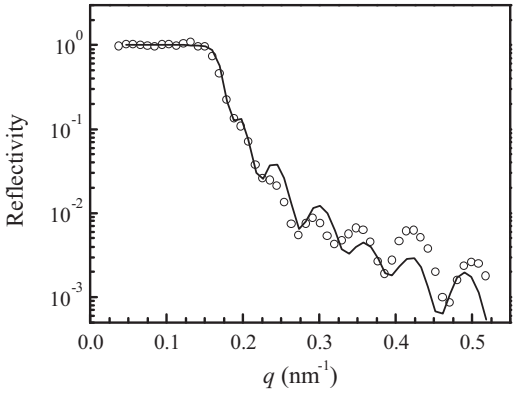

Fig. 4. Neutron reflectivity curve on Ta/$Mg_{70}Al_{30}$/Ta/Pd sample at 100 mbar fitted with a 5 layers model (with no gaps). This shows that this model could not fit the experimental data near saturation.

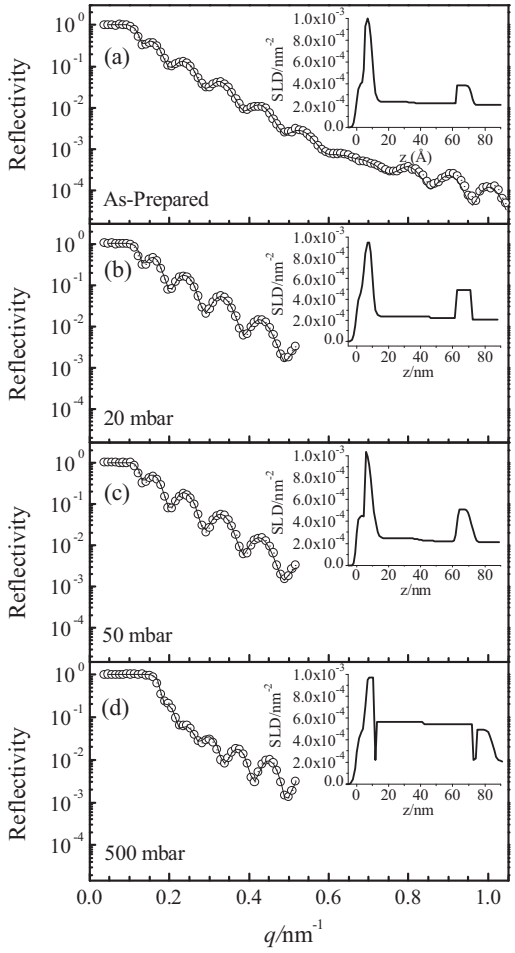

Fig. 5. Neutron reflectivity curves and corresponding SLD profiles of the Ta/$Mg_{70}Al_{30}$/Ni/Pd sample: (a) as prepared, and at D_2 pressures of: (b) 20 mbar, (c) 50 mbar, and (d) 500 mbar.

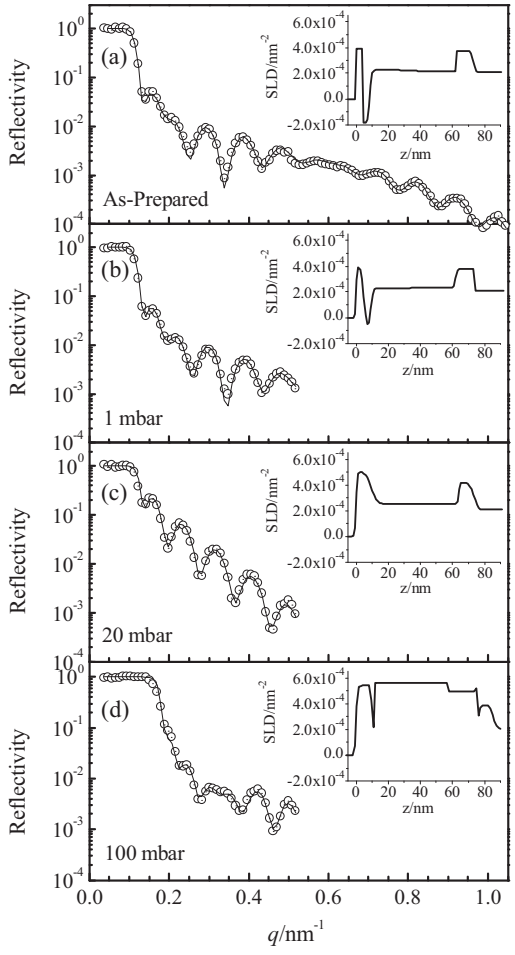

Fig. 6. Neutron reflectivity curves and corresponding SLD profiles on the Ta/$Mg_{70}Al_{30}$/Ti/Pd sample: (a) as prepared, and at D_2 pressures of: (b) 1 mbar, (c) 20 mbar, and (d) 100 mbar.

the SLD in the hydrogen containing $Mg_{70}Al_{30}$ phase reaches about 5.3×10^{-4} nm^{-2} or $D/M = 1.3$ and the whole layer has expanded by about 21%, i.e. from 52 nm (as-prepared) to 63 nm. The kinetics is relatively fast at 500 mbar, with most of the deuterium absorbed after about 1 h. The absorption process is accompanied by devoid gaps of about 2 nm on both sides of the $Mg_{70}Al_{30}$ layer, as noted on the previous sample. Further increase of the D_2 pressure up to 1 bar did not lead to any further increase of the hydrogen content in the film. It could be emphasized that, in contrast to the previous Ta catalyst layer, the Ni catalyst layer did not absorb deuterium at any stage during the experiment, in accordance with reported bulk Ni hydrogen absorption properties under the current (P,T) conditions [24].

3.1.3. $Mg_{70}Al_{30}$/Ti/Pd

Reflectivity curves and SLD profiles of the $Mg_{70}Al_{30}$/Ti/Pd sample are presented in Fig. 6 for increasing D_2 pressures. Fig. 6a shows the results obtained on the as-prepared $Mg_{70}Al_{30}$/Ti/Pd sample. The SLD values were found, as for the previous samples, in agreement with expected ones from tabulated data. The dip in the SLD profile observable around 5 nm is due to the negative coherent scattering length of titanium. Following deuterium introduction over the 1–20 mbar range (Fig. 6b and c), the sample absorbs deuterium mainly in the top Ti/Pd bilayer. The Ti layer, in particular, absorbs visibly significant amounts of deuterium in this low pressure range, with a SLD increasing from -1.9×10^{-4} nm^{-2} to 4.9×10^{-4} nm^{-2}. The latter value corresponds to a deuterium to metal ratio $D/M = 1.8$, which is very close to the stochiometric ratio for titanium hydride ($H/M = 1.97$) [25]. Such rapid absorption in the Ti layer is consistent with other observations.[15] The high affinity of Ti for hydrogen/deuterium possibly explains this important absorption at such low pressure; Ti has an enthalpy of formation of $\Delta_f H = -164$ kJ/mol, more than twice that of Mg (−74.5 kJ/mol) [25]. Small but observable amounts of deuterium are also found in the main $Mg_{70}Al_{30}$ phase with an SLD of about 2.5×10^{-4} nm^{-2} or $D/M \approx 0.1$. Significant absorption is observed in the $Mg_{70}Al_{30}$ layer around 100 mbar (Fig. 6d) where the SLD reaches 5.3×10^{-4} nm^{-2} or $D/M = 1.3$. This ratio is reached after about 7.5 h at this pressure, a time comparable to the Ta/Pd-catalyzed material at the same pressure. Further increase of the pressure lead to incremental changes in the SLD, the latter ultimately reaches about 5.5×10^{-4} nm^{-2} or $D/M = 1.32$ at 1 bar. The whole $Mg_{70}Al_{30}$ layer has ultimately expanded by about 23%, i.e. from 54 nm (as-prepared) to 66 nm. Gaps devoid of deuterium of about 2 nm are observable on each side of the $Mg_{70}Al_{30}$ layer.

3.1.4. $Mg_{70}Al_{30}$/Ta/Ni

The influence of the top catalyst layer was also investigated on another sample in which Ni was used as the top layer catalyst, i.e. a Ta/$Mg_{70}Al_{30}$ sample capped with a Ta/Ni top bilayer. The resulting NR curve and SLD profile are shown in Fig. 7. In this case, the D_2 pressure was increased up to 8 bar at room temperature. The resulting curves were found to be exactly the same as the as-prepared material, showing that no deuterium was absorbed in this sample.

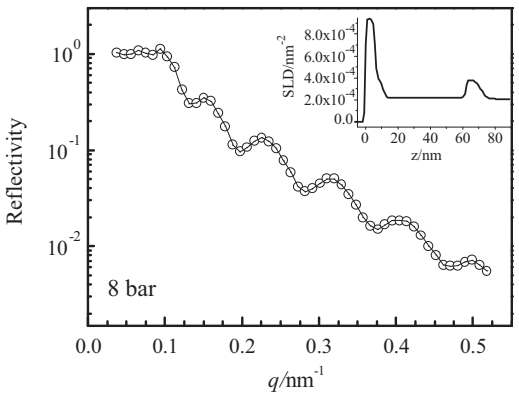

Fig. 7. Neutron reflectivity curve and corresponding SLD profiles on a $Ta/Mg_{70}Al_{30}/Ta/Ni$ sample at 8 bar D_2 at room temperature.

This result obtained using a Ta/Ni bilayer only confirms the effectiveness of Pd as a dissociation catalyst on the previous samples.

3.2. X-ray reflectometry

XRR measurements were performed on the same deuterium-exposed films used in the previous NR measurements. The XRR measurements were performed about 2 months after the NR experiments. Fig. 8a and b shows the XRR curves for the Ta/Pd and Ni/Pd-catalyzed materials, and the corresponding SLD profiles as modeled using four layers slab models. The simple model was found to fit the measured reflectivity curves well. The deduced $Mg_{70}Al_{30}$ layer thicknesses, in the 60–62.5 nm range, are the same as the ones obtained from NR measurements confirming the large expansion of this layer upon deuterium absorption. In contrast to NR, the XRR measurements do not show gaps in the SLD profile at the $Mg_{70}Al_{30}$ interfaces. As hydrogen and deuterium are nearly invisible for X-rays because of their low scattering lengths, these XRR measurements confirm that the metal interfaces are still intact after the deuterium absorption and that no metal interdiffusion is taking place. Hence, from this perspective, the devoid gaps and the concentration gradients observed in the previous neutron SLD profiles are only due to changes, in time, of the deuterium distribution in the films.

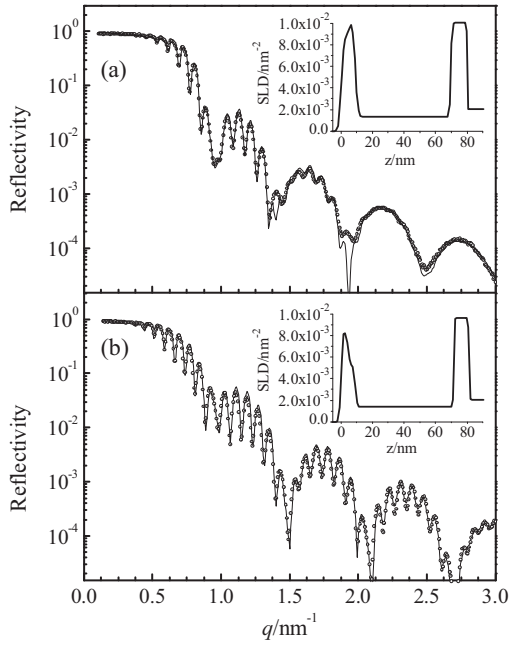

Fig. 8. X-ray reflectivity curves measured on the set of samples after about 60 days following D_2 exposure. (a) $Ta/Mg_{70}Al_{30}/Ta/Pd$ and (b) $Ta/Mg_{70}Al_{30}/Ni/Pd$.

3.3. X-ray diffraction (XRD)

From XRD measurements, we were able to detect the α-MgD_2 (1 1 0) peak at $2\theta = 27.9^\circ$ in the sample with the Ni/Pd catalyst, the other samples did not show any hydride peaks. That means that the samples with the Ta/Pd and Ti/Pd bilayer desorbed over the 2 months at room temperature.

4. Discussion

The present observations show that the absorption mechanism involves first the absorption of deuterium in the catalyst layers, followed by the absorption in the main $Mg_{70}Al_{30}$ layer. Some deuterium observed early in the bottom Ta layer reveals atomic deuterium has been transported through the Mg alloy phase without accumulating in it. These observations are consistent with a reduction of the dissociation barriers due to the bilayer catalysts, and suggest a spillover mechanism. The $Mg_{70}Al_{30}$ phase on all three samples consistently absorbed up to D/M values between ~1.30 and 1.35. From a stoichiometric standpoint, such uptakes are compatible with the formation of a MgD_2 phase, considering the 70% Mg content of the alloy. The slow formation of this phase in all cases suggests a significant nucleation barrier for the formation of MgD_2. In fact, the $Mg_{70}Al_{30}$ layers on the different samples have expanded by up to 23% after saturation, implying a considerable work associated with deuteride formation. Near saturation, it was found that the usual four (or five) layer model could not fit the experimental data, and that gaps in the SLD profiles at the $Mg_{70}Al_{30}$ interfaces had to be introduced to get a good fit. The presence of these gaps, which extend within the 1–2.5 nm range, indicates the presence of poorly or non-absorbing metallic phases. Compressive stress at the interface, known to be detrimental to hydrogen solubility [26], may prevent the formation of MgD_2 in these regions. It should be noted that these gaps were not visible using the XRR, supporting the assumption that they truly result from a deuterium depletion only revealed by neutrons. The presence of such gaps is qualitatively consistent with observations made by another team on comparable samples [27].

A comparison of the absorption pressures on the different samples shows that the Ta- and Ti-catalyzed films behave similarly as they both absorb most of the deuterium at the lowest pressures ($p \cong 100$ mbar), and with similar kinetics. These two metals, which are poorly miscible in Mg, may offer elastically disconnected interfaces favoring the formation of MgD_2 [27]. The easy deuteration of the Ti layer at low pressures is consistent with a high affinity for deuterium. In contrast, exposure of the Ni-catalyzed sample to 100 mbar D_2 did not lead to observable deuteration, revealing much slower kinetics at this pressure comparatively to the other samples. As mentioned previously, this sample required $p \cong 500$ mbar to fully absorb. It could be noted that Ni alloys easily with Mg and that may be at the origin of elastic constraints potentially detrimental to the formation of MgD_2 at interfaces [27]. On the other hand, XRD measurements showed that the Ni-containing sample, unlike the other samples, still had deuterium absorbed in it more than 60 days after the in situ experiments. These results suggest Ni may act like a diffusion barrier to both absorption and desorption in the present sample, implying a symmetry in the two mechanisms. These results somewhat contrast with some findings by Pasturel et al. [15] from which no significant differences in the hydrogenation time can be extrapolated for very small interlayers made of different metals. But then again, the present results are consistent

with the longer dehydrogenation times obtained using a Ni interlayer [15]. It is interesting to note that all the current samples have absorbed at much lower pressure than a $Mg_{70}Al_{30}$ sample catalyzed with a single (10 nm) Pd layer, which required a pressure of ~1.3 bar to fully absorb deuterium at room temperature [11].

5. Conclusions

The absorption mechanism on $Mg_{70}Al_{30}$ thin films catalyzed with different metal bilayers was investigated using neutron reflectometry. The presented experiments clearly evidenced, in a nanoscale representation, a two-steps mechanism involving absorption in the catalyst followed by spillover in the $Mg_{70}Al_{30}$ layer and subsequent formation of MgD_2. Such mechanism was observed independently of the type of bilayer used, but the formation of MgD_2 occurred at different pressures dependent on the metal catalyst used. With respect to a single layer Pd catalyst, the current bilayer catalysts can help improve the hydrogen absorption properties of such films while reducing by half the Pd content. In particular, it was found that the Ti/Pd catalyzed material offers the milder absorption conditions, i.e. saturation at 100 mbar at room temperature, and an improved total hydrogen uptake. Finally, the measurements have revealed the presence of gaps devoid of deuterium at $Mg_{70}Al_{30}$ interfaces near saturation, a possible result of compressive stress at the same interfaces. In future works, absorption and desorption properties on these materials will be investigated at higher temperatures, where usable pressures can be obtained and thermodynamics can be investigated.

References

[1] B. Sakintuna, F. Lamari-Darkrim, M. Hirscher, Int. J. Hydrogen Energy 32 (9) (2007) 1121–1140.
[2] J. Huot, G. Liang, R. Schulz, Appl. Phys. A 72 (2) (2001) 187–195.
[3] A. Zaluska, L. Zaluski, J.O. Ström-Olsen, J. Alloys Compd. 288 (1999) 217–225.
[4] V. Bérubé, G. Radtke, M. Dresselhaus, G. Chen, Int. J. Energy Res. 31 (6–7) (2007) 637–663.
[5] M.A. Pick, J.W. Davenport, M. Strongin, G.J. Dienes, Phys. Rev. Lett. 43 (4) (1979) 286–289.
[6] Ch. Rehm, H. Fritzsche, H. Maletta, F. Klose, Phys. Rev. B 59 (4) (1999) 3142–3152.
[7] S. Singh, S.W.H. Eijt, M.W. Zandbergen, W.J. Legerstee, V.L. Svetchnikov, J. Alloys Compd. 441 (1–2) (2007) 344–351.
[8] F. Tang, T. Parker, H.-F. Li, G.-C. Wang, T.-M. Lu, Nanotechnology 19 (46) (2008) 465706.
[9] R. Gremaud, A. Borgschulte, C. Chacon, J.L.M. Van Mechelen, H. Schreuders, A. Züttel, B. Hjörvarsson, B. Dam, R. Griessen, Appl. Phys. A 84 (1–2) (2006) 77–85.
[10] A.J. Du, S.C. Smith, X.D. Yao, G.Q. Lu, J Am. Chem. Soc. 129 (33) (2007) 10201–10204.
[11] C.T. Harrower, E. Poirier, H. Fritzsche, P. Kalisvaart, S. Satija, B. Akgun, D. Mitlin, Int. J. Hydrogen Energy 35 (19) (2010) 10343–10348.
[12] R. Domenèch-Ferrer, M.G. Sridharan, G. Garcia, F. Pi, J. Rodríguez-Viejo, J. Power Sources 169 (1) (2007) 117–122.
[13] X. Tan, C.T. Harrower, B. Shalchi Amirkhiz, D. Mitlin, Int. J. Hydrogen Energy 34 (18) (2009) 7741–7748.
[14] H. Fritzsche, C. Ophus, C.T. Harrower, E. Luber, D. Mitlin, Appl. Phys. Lett. 94 (2009) 241901.
[15] M. Pasturel, R.J. Wijngaarden, W. Lohstroh, H. Schreuders, M. Slaman, B. Dam, R. Griessen, Chem. Mater. 19 (3) (2007) 624–633.
[16] H. Fritzsche, M. Saoudi, J. Haagsma, C. Ophus, E. Luber, C.T. Harrower, D. Mitlin, Appl. Phys. Lett. 92 (2008) 121917.
[17] H. Fritzsche, E. Poirier, J. Haagsma, C. Ophus, E. Luber, C.T. Harrower, D. Mitlin, Can. J. Phys. 88 (10) (2010) 723–728.
[18] Y. Song, Z.X. Guo, R. Yang, Phys. Rev. B 69 (9) (2004) 094205.
[19] C.X. Shang, M. Bououdina, Y. Song, Z.X. Guo, Int. J. Hydrogen Energy 29 (1) (2004) 73–80.
[20] X.L. Zhou, S.H. Chen, Phys. Rep. (Rev. Sec. Phys. Lett.) 257 (1995) 223–384.
[21] A. Nelson, J. Appl. Crystallogr. 39 (2006) 273–276.
[22] http://motofit.sourceforge.net/wiki/index.php/Main_Page.
[23] H. Kiessig, Ann. Phys. 402 (1931) 769–788.
[24] F.D. Manchester, Phase Diagrams of Binary Hydrogen Alloys, ASM International, Materials Park, OH, USA, 2000.
[25] http://hydpark.ca.sandia.gov.
[26] R.W. Cahn, P. Haasen, E.J. Kramer (Eds.), Electronic and Magnetic Properties of Metals and Ceramics Part II, VCH Publishers Inc., New York, NY, USA, 1994.
[27] A. Baldi, M. Gonzalez-Silveira, V. Palmisano, B. Dam, R. Griessen, Phys. Rev. Lett. 102 (2009) 226102.